Self-Assembled Multibilayers of Europium Alkanoates: Structure, Photophysics, and Mesomorphic Behavior

Haolong Li, Weifeng Bu, Wei Qi, and Lixin Wu*

Key Laboratory for Supramolecular Structure and Materials, Ministry of Education, Jilin University, Changchun 130012, People's Republic of China

Received: July 19, 2005; In Final Form: September 1, 2005

A series of europium alkanoates $(C_{n-1}H_{2n-1}CO_2)_3Eu$, ($n$ = 14, 16, 18, 20) have been synthesized and characterized in detail. X-ray diffraction and Fourier transform infrared spectroscopic measurements confirm the multibilayer structure of these homologues. In such bilayers, the europium ionic layers are well separated by the highly ordered alkyl chains which are in an all-trans conformation and perpendicular to both sides of the europium ionic layers. There is a mixed-coordination type of chelating bidentate and bridging bidentate between the carboxylate groups and the europium ions. All samples exhibit characteristic emission of europium, though the luminescent intensity has been partly quenched by the carboxylate groups. Differential scanning calorimetry (DSC) shows multiple melting points for these homologues, and temperature-dependent X-ray diffraction measurements also confirm the existence of the mesophase on heating. This mesophase is not truly liquid crystalline, but is similar to the smectic A phase of organic rodlike molecules. Meanwhile, it seems that with increasing atomic number of lanthanide ions, longer alkyl chains will be required to form such a mesophase for the corresponding lanthanide alkanoates.

Introduction

Materials with ordered structures always have particular properties due to the ordered arrangement of molecules, and low-dimensional layered assemblies are just a typical example that have been attracting much attention lately. Approaches for fabricating low-dimensional layered materials have been developed by applying the strategy from artificial Langmuir−Blodgett (LB) technique to the self-assembling method. As a result, a series of monolayer or multilayer assemblies have been obtained.[1] Recent reports have revealed that some metal complexes with long alkyl chains can self-assemble to lamellar structure through simply precipitating from the solution, such as metal thiolates and metal alkanoates.[1,2] This lamellar structure is attributed to the cooperative effect of the van der Waals interactions between the organic alkyl chains and the electrostatic interactions between the inorganic metal ions, in which the planes of metal ions are well separated by alkyl chain bilayers (see Scheme 1). The long alkyl chains can well maintain their integral layered structure even on heating, so an unusual thermal liquid crystal behavior always results.[2d,3]

Functional metal ions have been incorporated into such low-dimensional layered assemblies to realize new synergic properties. Especially for rare earth metal ions, because of their pure luminescence from narrow emission, efforts have been made to incorporate their excellent photophysical properties with the liquid crystal properties of low-dimensional layered materials.[4] Several lanthanide alkanoates have been studied in detail, such as those of cerium and neodymium. The results show that when the length of alkyl chains is increased, a thermal liquid crystal behavior goes from emergence to vanishing. Interestingly, for different lanthanide ions, the corresponding length range of alkyl chains that can bring about a thermal liquid crystal varies. Binnemans et al. have systematically studied the thermal behavior of lanthanide dodecanoates and have found that the ionic radius has a crucial effect on the formation of the mesophase.[5] The mesophase is observed for the dodecanoates with light lanthanide ions having large ionic radii, such as lanthanum, cerium, praseodymium, and neodymium, but not for the dodecanoates of heavy lanthanides, such as europium and terbium. The overall consideration is that there seems to be some regularity playing a role in the thermal liquid crystal phenomena. We assume that, for a lanthanide alkanoate, the higher the atomic number of the lanthanide, the longer the length of alkyl chains that will be required to form a mesophase. With this hypothesis, we have synthesized a series of europium *n*-alkanoates, $(C_{n-1}H_{2n-1}CO_2)_3Eu$ (n = 14, 16, 18, 20), and named them $C_{14}Eu$, $C_{16}Eu$, $C_{18}Eu$, and $C_{20}Eu$, respectively. The subsequent characterizations confirm our supposition. These europium alkanoates exhibit multiple melting points starting from $C_{14}Eu$, which cannot be observed for $(C_{11}H_{23}CO_2)_3Eu$ according to previous reports,[5] and the multiple melting points began to unite

SCHEME 1: Layered Structure of Long-Chain Metal Thiolates or Metal Alkanoates

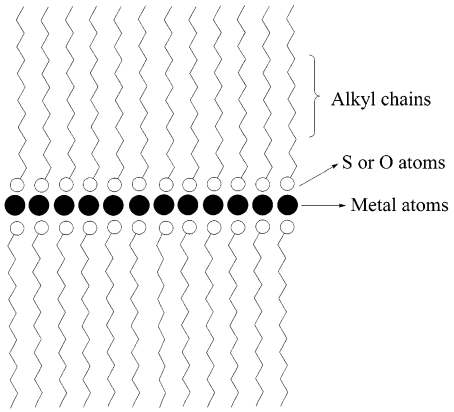

* Corresponding author. E-mail: wulx@jlu.edu.cn.

10.1021/jp053980o CCC: $30.25
Published on Web 10/21/2005

into one melting point with the increasing length of alkyl chains. This finding reflects the relationship between the formation of mesophase and the length of alkyl chains, which is helpful to further comprehending the mesophase of lanthanide alkanoates and will provide some guidance for the design of lanthanide-containing liquid crystal display devices.

Experimental Section

The approach to preparing the metal alkanoates follows two normally used methods.[5,6] The experimental details are shown below. All chemicals were used as received with purity higher than 99.9%.

Synthesis of Potassium *n*-Alkanoate ($C_{n-1}H_{2n-1}CO_2K$, $n = 14, 16, 18, 20$). An aqueous solution of KOH (0.56 g, 0.01 mol) in water (5 mL) was diluted with acetone (30 mL) and added dropwise to a stirred solution of *n*-alkanoic acid (0.01 mol) in acetone (50 mL). Then the mixture was heated to reflux for 3 h. After cooling to room temperature, the white precipitate of potassium *n*-alkanoate was filtered, washed repeatedly with hot acetone, and dried in a vacuum at room temperature for 12 h (yield > 90%).

Synthesis of Europium *n*-Alkanoate ($(C_{n-1}H_{2n-1}CO_2)_3Eu$, $n = 14, 16, 18, 20$). Potassium *n*-alkanoate (0.006 mol) was dissolved in a mixture of deionized water and ethanol (50 mL, 1:1 v/v) and added dropwise to a stirred solution of $Eu(NO_3)_3 \cdot 6H_2O$ (0.002 mol) in deionized water (10 mL). A white precipitate formed immediately, and then the mixture was stirred at room temperature for 3 h. Subsequently, the precipitate was filtered, and washed repeatedly with aqueous ethanol (1:1 v/v) and hot acetone to remove the residual europium salt and potassium soap. A white powder was obtained and dried at room temperature for 24 h to give the products (yield > 85%).

In all samples, water molecules are contained, which were detected by differential scanning calorimetry (DSC) and thermogravimetric analysis (TGA) measurements. For each europium alkanoate, the first heating curve of DSC shows a strong endothermal peak in the range of 80−120 °C, and this peak disappeared in the second heating curve, indicative of the loss of water. Meanwhile, the TGA curve also shows a subtle descendent inflection at the same temperature range. The weight losses (%) at about 120 °C are the following: 2.02 for $C_{14}Eu$, 2.22 for $C_{16}Eu$, 1.98 for $C_{18}Eu$, and 2.07 for $C_{20}Eu$. From this, it can be deduced that each europium alkanoate molecule contained 0.5−1 water molecule. Their purities are further confirmed by elemental analysis (EA). Calcd (%) for $(C_{13}H_{27}CO_2)_3Eu \cdot H_2O$ (852.07): C 59.20, H 9.82. Found: C 59.43, H 10.04. Calcd (%) for $(C_{15}H_{31}CO_2)_3Eu \cdot H_2O$ (936.23): C 61.58, H 10.23. Found: C 61.83, H 10.28. Calcd (%) for $(C_{17}H_{35}CO_2)_3Eu \cdot H_2O$ (1020.39): C 63.56, H 10.57. Found: C 63.72, H 10.65. Calcd (%) for $(C_{19}H_{39}CO_2)_3Eu \cdot 0.5H_2O$ (1095.54): C 65.78, H 10.86. Found C 65.94, H 10.91.

These powders were also examined by scanning electron microscopy (SEM) and were found to be a typical cobble-shaped plate tens of nanometers wide (see Figure 1).

Measurements. Elemental analysis (C, H) was measured on a Flash EA1112 analyzer from ThermoQuest Italia S.P.A. Fourier transform infrared (FT-IR) spectra were performed on a Bruker IFS66V FT-IR spectrometer equipped with a DGTS detector (32 scans), using KBr pellets, and the spectra were recorded with a resolution of 4 cm^{-1}. Luminescent measurements were performed on a Spex FL=2T2 spectrophotometer using a xenon lamp as the excitation source. Temperature-dependent X-ray diffraction (XRD) was carried out on a Rigaku X-ray diffractometer (D/max 2500 V, using Cu Kα radiation at a wavelength of 1.5416 Å) with a PTC-20A temperature controller (temperature range from −180 to 800 °C). The data were collected in the range (2θ) from 1.5° to 35°. Room-temperature X-ray diffraction was measured on a Rigaku X-ray diffractometer (D/max rA, using Cu Kα radiation at a wavelength of 1.542 Å), and the data were collected separately in the lower angle range from 0.7° to 10° and in the higher angle range from 10° to 46°. DSC measurements were performed on a Netzsch DSC 204 calorimeter at a scanning rate of 10 °C·min^{-1}. Optical textures of the mesophase were studied with a polarized optical microscope (Leica DMLP, Germany). TGA was measured on a Perkin-Elmer 7 series thermal analysis system. Scanning electron microscopy was made with a FET XL30 ESEM FEG instrument.

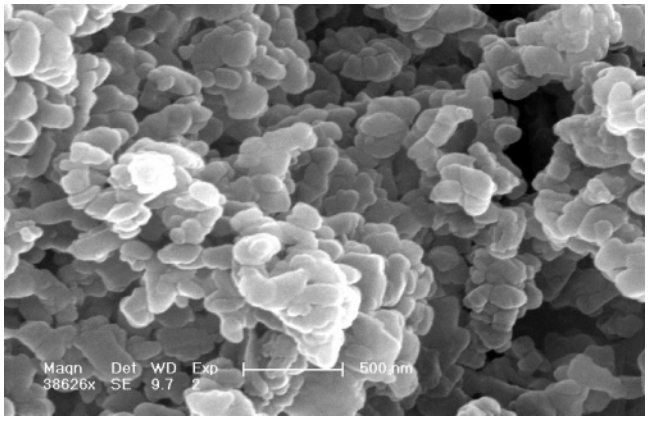

Figure 1. Morphology of the powder of $C_{14}Eu$ observed by scanning electron microscopy.

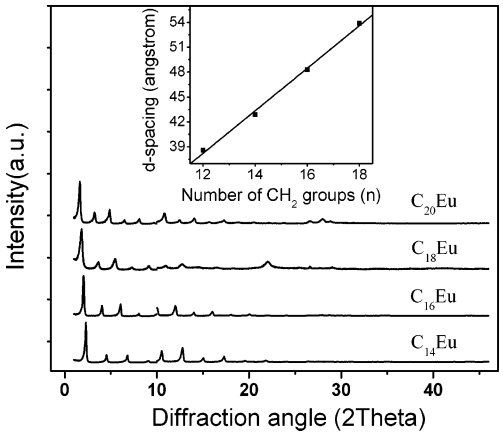

Figure 2. X-ray diffraction patterns of the four europium alkanoates at room temperature. The inset is the linear fitting of the interlayer distances as a function of the number of CH_2 groups ($r = 0.9983$).

Results and Discussion

Multibilayer Structure of Europium Alkanoates. Room-temperature XRD analysis of these europium alkanoates affirms the presence of a lamellar structure. All the compounds show progressional reflections in the low-angle region (Figure 2), which are successive orders of diffractions from the layered structure with a certain *d* spacing. There are also weak diffractions in the high-angle region due to the ordered intralayer structure. These diffraction patterns can be interpreted in terms of three-dimensionally stacked planes of europium atoms which are separated from each other by the bilayer of alkyl chains, just like the typical metal complex containing long alkyl chains. The calculated *d* spacing values are in the ratio of

TABLE 1: Assignment of Vibration Modes in IR Spectra of the Four Samples

number of C atoms (n)				
14	16	18	20	vibr assignt
2957	2957	2957	2957	$\nu_{as}(CH_3)$
2918	2918	2918	2918	$\nu_{as}(CH_2)$
2874	2874	2874	2874	$\nu_s(CH_3)$
2848	2848	2848	2848	$\nu_s(CH_2)$
1532	1532	1530	1532	$\nu_{as}(COO)$
1468	1467	1467	1468	$\delta(CH_2)$
1456	1456	1453	1454	$\delta_{as}(CH_3)$
1413	1410	1416	1412	$\nu_s(COO)$
1379	1379	1379	1379	$\delta_s(CH_3)$
1110	1108	1109	1107	$\nu(C-C)$
943	941	942	940	$\nu(C-C)COO$
721	721	721	721	$\rho(CH_2)$
683	684	686	685	$\delta(COO)$

1:1/2:1/3:...:1/n, and these patterns are indexed as (00l) Bragg reflections. The deduced interlayer distances from the experimental results (D_{exp}) are 38.58, 42.89, 48.28, and 53.87 Å for $C_{14}Eu$, $C_{16}Eu$, $C_{18}Eu$, and $C_{20}Eu$, respectively. These distances are plotted as a function of the chain length of each material (see the inset of Figure 2), and the good linear correlation indicates that these materials share a common structure. The slope observed (S_{obs}) is 2.56 Å per pair of CH_2 groups, similar to the ideal model (2.54 ± 0.02 Å per pair of CH_2 groups, based on a survey of XRD data from a larger number of ordered alkyl chain crystals),[1c] in which the alkyl chains are fully extended and are in an all-trans conformation. Furthermore, the tilt angle of the chains can be estimated from the formula as $\theta = \cos^{-1}(S_{obs}/2.54)$, and the calculated value is 0°. Thus, we can confirm that the alkyl chains in our samples are perpendicular to the central europium ionic layer.

The y-intercept is 7.46 Å, which represents the thickness of the central layer (the spacing between the carbon atoms of the first CH_2 groups on either side of the central europium plane) plus the spacing between CH_3 groups of adjacent layers, and the latter may be minus if interdigitation between alkyl chains exists.[1c] The maximal interlayer distance (D_{max}) in ideal modes can be calculated by the formula $D_{max} = 2d_{C-H} + 2(n-1)d_{C-C}(\sin 55°) + 2d_{C-O} + 2r_{Eu^{3+}}$, where n = total number of carbon atoms, $d_{C-H} = 1.09$ Å, $d_{C-C} = 1.54$ Å, $d_{C-O} = 1.36$ Å, and $r_{Eu^{3+}} = 0.95$ Å.[4a] The obtained D_{max} values are 39.60, 44.65, 49.70, and 54.74 Å for $C_{14}Eu$, $C_{16}Eu$, $C_{18}Eu$, and $C_{20}Eu$, respectively. It can be seen that the D_{max} values are all similar to the corresponding D_{exp} ones (see above); these agreements give further support that the alkyl chains are in all-trans conformation.

As an effective measurement, infrared spectroscopy has been used extensively for the study of long alkyl chain systems, such as alkanol and alkanoic acids monolayer on metal surfaces,[7a,b] metal thiolates,[1c,2a] bulk alkanes,[7c] and phospholipid bilayers.[7d] It is also suitable for our system.[2d] All four samples have been investigated by FT-IR measurement, and the detailed assignments of the bands are summarized in Table 1.

Figure 3A shows the C−H stretching modes in the high-frequency region from 2800 to 3000 cm^{-1}. For crystalline alkanes, the symmetric (d^+) and antisymmetric (d^-) modes of CH_2 appear at 2847 ± 1 cm^{-1} and 2916 ± 1 cm^{-1}, which represent the extremely high percentage of all-trans conformations. When the disordered conformation of alkyl chains increases, these peaks shift to higher frequencies.[8] In our samples, the d^+ and d^- modes appear at 2849 and 2918 cm^{-1}, respectively. It is a typical behavior of highly ordered crystalline bulk alkyl chains and also consistent with the conclusion from XRD results. For the CH_3 modes, their symmetric (r^+) and antisymmetric (r^-) values are at 2874 and 2957 cm^{-1}, respectively, similar to the alkyl chains whose termini are in a semifrozen state.[2a] Furthermore, the rotational freedom of the chain terminus can be evaluated from the splitting of the r^- mode. This splitting indicates the decreasing symmetry of the CH_3 as a result of the intermolecular interactions between the alkyl chains. By contrast, the degeneration of this splitting into a single peak in our samples shows that the CH_3 group should be in at least a C_3 symmetry.[2a,9] Seen from the XRD results, the alkyl chains do not interdigitate; their tail-to-tail stacking mode is somewhat loose and may be helpful to maintain the symmetry of the terminal CH_3 group. In addition, the intensity ratio of I_{2849}/I_{2918} has often been used as diagnostic of the alkyl chain arrangement.[8] When the conformational order of alkyl chains increases, this ratio increases, too.[2a] Figure 3B shows a plot of I_{2849}/I_{2918} versus numbers of CH_2 groups. It can be seen that this ratio increases with increasing length of alkyl chains, implying that the conformational order is increasing, which can be regarded as a result of the increasing van der Waals interactions in the longer chains. When the number of CH_2 groups has increased to 16, the alkyl chains seem almost in a crystal state, which represents the high point of ordered conformation, so the increasing tendency of I_{2849}/I_{2918} becomes slower than that with short alkyl chains.

Figure 4 shows the low-frequency region of the samples between 600 and 1800 cm^{-1}. The absorption bands in this region are mostly composed of the scissoring, wagging, twisting, and rocking modes of the CH_2 group and the stretching mode of the COO^- group. These bands are progressional and highly coupled, which is a characteristic of alkyl chains in all-trans conformation. The detailed assignments of all the bands are summarized in Table 1. Herein, the strong single band appearing about 1468 cm^{-1} is the scissoring (δ) mode of CH_2 and has been widely used to investigate the packing arrangement of alkyl chains. In general, the alkyl chains mainly have three kinds of crystalline packing: triclinic, orthorhombic, and hexagonal. The triclinic packing gives a strong, narrow and sharp single $\delta(CH_2)$ band at 1470−1474 cm^{-1}, the orthorhombic packing gives a doublet $\delta(CH_2)$ band at ∼1462 and ∼1474 cm^{-1}, and the hexagonal packing gives a single $\delta(CH_2)$ band at 1468−1469 cm^{-1}.[10,11] In comparison with the three cases, the alkyl chains of the present samples are in a state similar to hexagonal packing. On the other hand, the single band around 721 cm^{-1} of all samples is assigned to the in-plane rocking (ρ) mode of CH_2 group, and it appears for the crystalline compounds with more than four consecutive CH_2 groups.[12] The shapes of $\delta(CH_2)$ and $\rho(CH_2)$ bands are both highly dependent on the packing geometry of the alkyl chains. In polyethylene and bulk alkanes, these bands split due to the intermolecular interactions between the adjacent CH_2 groups of the two chains in a crystal subcell.[12,13] In the present cases, all samples show a singlet for both two bands around 1467 and 721 cm^{-1}, indicating that there is only one chain in a hexagonal unit cell.

Generally speaking, the bands of out-of-plane and in-plane CH_3 asymmetric deformation modes appear at 1455 and 1460 cm^{-1}, respectively, and their envelopment will lead to a broad shoulder about 1456 cm^{-1}. All spectra of our samples exhibit a shoulder about 1455 cm^{-1}, which should result from an effect of band envelopment, just like the description above. Because of their similar spectral characteristics, we believe these homologues should possess the same alkyl chain conformation. However, there is still a remarkable difference between the numbers of CH_2 wagging progression bands in IR spectra due

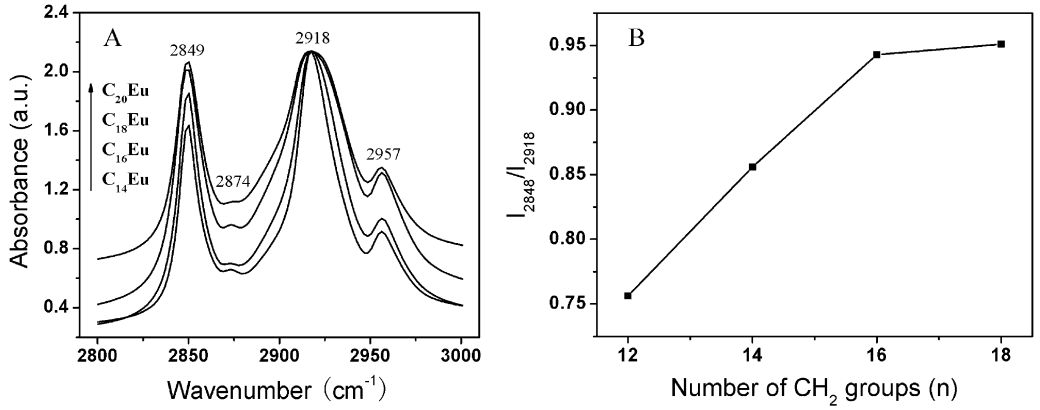

Figure 3. (A) FT-IR spectra of C_{14}Eu, C_{16}Eu, C_{18}Eu, and C_{20}Eu (from bottom to top) in high-frequency region. Each spectrum has been normalized to the same peak at 2918 cm^{-1} for convenient contrast. (B) Plot of I_{2849}/I_{2918} versus number of CH_2 groups.

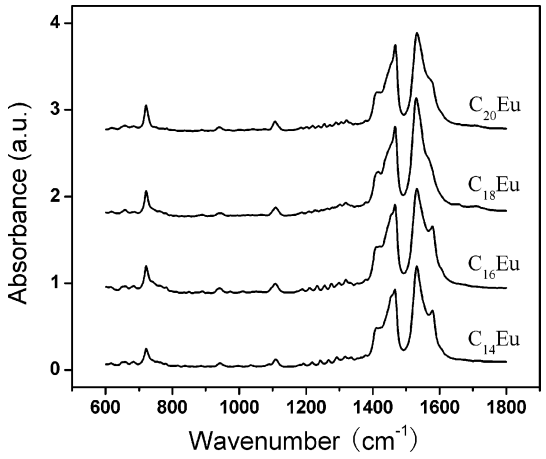

Figure 4. FT-IR spectra of C_{14}Eu, C_{16}Eu, C_{18}Eu, and C_{20}Eu (from bottom to top) in low-frequency region.

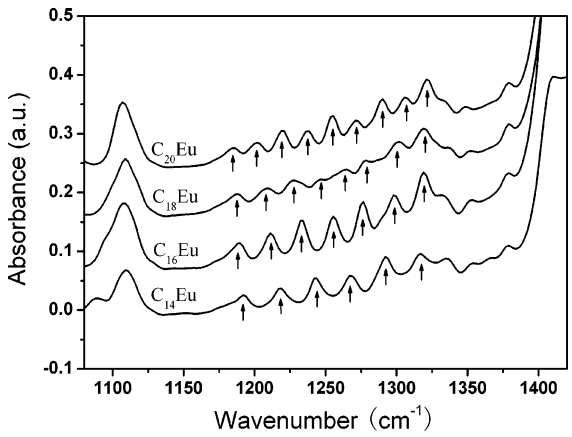

Figure 5. FT-IR spectra of C_{14}Eu, C_{16}Eu, C_{18}Eu, and C_{20}Eu (from bottom to top). Wagging modes of CH_2 groups are indicated by black arrows.

to the different lengths of the alkyl chains among the homologues, which are observable in the region of 1350−1150 cm^{-1}. For an even-numbered chain, the number of CH_2 wagging bands is equal to $m/2$ (m is the number of carbon atoms of CH_2 groups); for an odd-numbered chain, the number of these bands is $(m + 1)/2$.[14,15] In Figure 5, the number of these bands is indicated, and their values are 6, 7, 8, and 9 for C_{14}Eu, C_{16}Eu, C_{18}Eu, and C_{20}Eu, respectively, consistent with the $m/2$ carbon atoms of CH_2 groups contained in each sample. Meanwhile, the clear and well-separated shapes of these bands also indicates that the alkyl chains are in all-trans conformation.

Coordination and Photophysical Properties of Europium Alkanoates. For the IR spectra of long-chain aliphatic acids, there is a single band around 1700 cm^{-1} due to the antisymmetric C═O stretching mode.[16] When the carboxyl group interacts with metal, this singlet disappears and splits into a doublet, corresponding to the antisymmetric and symmetric stretching modes, respectively, of the formed carboxylate group. In some reports, the frequency separation $\Delta\nu = \nu_{as}(COO) - \nu_s(COO)$ is applied as evidence to elucidate the coordination type of metal carboxylates.[11,17] There are mainly three coordination types between metal and carboxylate group—monodentate, chelating bidentate, and bridging bidentate—as shown in Scheme 2. Monodentate coordination removes the equivalence of the C═O bond, resulting in an increase in $\nu_{as}(COO)$ and a decrease in $\nu_s(COO)$, and the corresponding $\Delta\nu$ becomes relatively large, up to 200−400 cm^{-1}.[2d] For the present cases, the $\nu_{as}(COO)$ and $\nu_s(COO)$ both shift to low frequency, appearing at 1532−1530 and 1410−1416 cm^{-1}, respectively. Therefore, the existence of monodentate coordination seems impossible and there should be a bidentate coordination in the four samples. It has been found that both chelating bidentate coordination and bridging bidentate coordination can coexist in the crystals of neodymium butyrate[18] and the powders of cobalt(II) soap $[Co\{CH_3(CH_2)_{10}COO\}_2(H_2O)_2]$.[6] All $\Delta\nu$ values of our samples are about 120 cm^{-1}, just falling in the $\Delta\nu$ range between chelating bidentate coordination (40−80 cm^{-1}) and bridging bidentate coordination (140−170 cm^{-1}), and similar to the $\Delta\nu$ of 128 cm^{-1} for cobalt(II) soap mentioned above. Thus, it is very possible that a mixed-coordination type of chelating and bridging exists in our samples. In such case, the europium ions not only interact with carboxylate groups through chelating bidentate or bridging bidentate coordination, but also act as connecters between the adjacent carboxylate groups in the bridging type (see Scheme 2). Such a structure can form a robust and intraconnected central layer of europium ions, and the alkyl chains are grafted to this layer. Viewed from the point of structural stability, this structure is more helpful for maintaining the whole lamellar structure upon heating.

As is well-known, the luminescence of europium complex is sensitive to the microenvironment of Eu^{3+}, especially to the coordination environment. Figure 6 shows the excitation and emission spectra of C_{16}Eu, which exhibit the characteristic luminescence of europium. In the excitation spectra, the bands at 398, 384, 379, 364, and 321 nm are attributed to the transitions of $^7F_0 \rightarrow {}^5L_{6,7,8}$, $^7F_0 \rightarrow {}^5D_4$ and ^5H multiplet, and the bands at 468 and 419 nm are assigned to the transitions of $^7F_0 \rightarrow {}^5D_2$ and $^7F_1 \rightarrow {}^5D_3$.[19] In the emission spectra, the bands at 578, 591, 613 and 619, 651, 691, and 698 nm are attributed to the

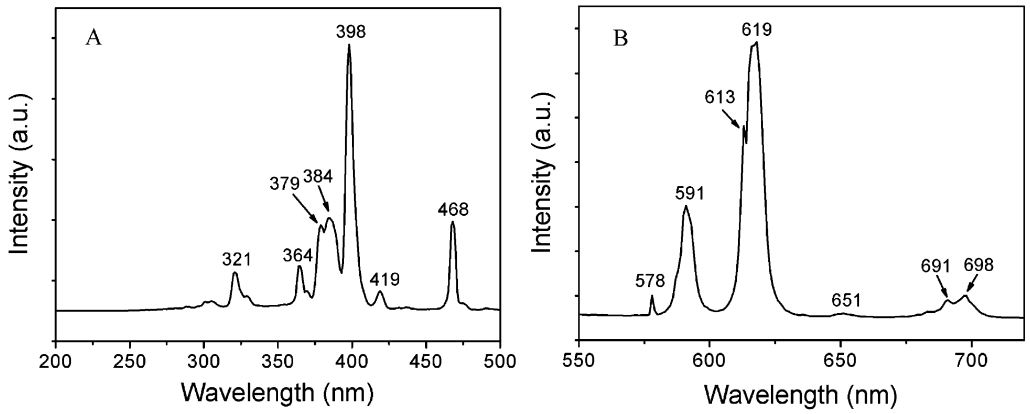

Figure 6. Excitation (A, monitored at 619 nm) and emission (B, monitored at 398 nm) spectra of $C_{16}Eu$ powders at room temperature.

SCHEME 2: Three Main Coordination Types in Metal Carboxylates, Where the Metal Atom Is Denoted by "M"

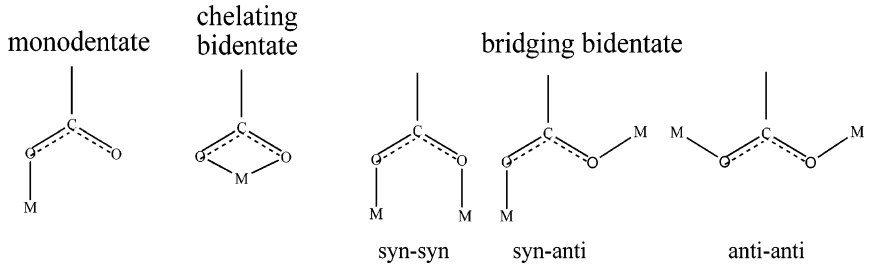

transitions of $^5D_0 \rightarrow {}^7F_{0,1,2,3,4}$.[20] The symmetrically forbidden transition at 578 nm is clearly observed as a single peak, indicating that the symmetry of the Eu^{3+} site is probably in C_{nv}, C_n, or C_s symmetry.[21] The other three homologues show photophysical properties similar to those of $C_{16}Eu$, and the corresponding fluorescent spectra are available in the Supporting Information. The similar results imply that the length of alkyl chains cannot remarkably affect the luminescence of the central Eu^{3+} plane, at least in the number range of CH_2 groups from 12 to 18. Unfortunately, compared with that of $Eu(NO_3)_3$, the emissive intensities of the present europium alkanoates decrease greatly. The intense red luminescence of $Eu(NO_3)_3$ under ultraviolet excitation is not observed for europium alkanoates under the same condition. This may result from the quenching of the carboxylate groups, for the excited 5d electrons of Eu^{3+} can partially decay to the closely lying π^* orbital of the ligand and thus cannot fall back to the ground state through radiative transitions, as has been reported in similar cases of other luminescent metal carboxylates.[22]

Thermal Behavior of Europium Alkanoates. The thermal behavior of these homologues has been investigated by differential scanning calorimetry (DSC), heat-stage polarized optical microscopy, and temperature-dependent X-ray diffraction. In Binnemans's work on lanthanide(III) dodecanoates, the mesophase can only form for the light lanthanide elements with a large ionic radius such as La(III), Ce(III), Pr(III), and Nd(III), but not for the heavy lanthanides. For example, europium dodecanoate exhibits only a single melting point at 90 °C.[5] However, for the present four europium alkanoates, obvious mesophases upon heating are shown, and more than one melting point can be seen in the DSC thermograms, such as $C_{16}Eu$, whose thermogram is shown in Figure 7. In the first heating process of each sample, there is a strong endothermal peak before the melting points due to the loss of water, and this peak disappears in the reheating process. In the subsequent heating or cooling cycles, the DSC curves can be well repeated. All samples exhibit supercooling as often observed in ionic metallomesogens, indicating that the mesophases are not truly liquid crystalline but still have a considerable degree of crystalline order.[2d] The phase transition temperatures during the first cooling and second heating process, and the corresponding enthalpies and entropies of all the samples are summarized in Table 2. From these results, we have observed an interesting tendency that the multiple melting points can gradually incorporate into one melting point from $C_{14}Eu$ to $C_{20}Eu$. For $C_{14}Eu$, there are three melting points during the heating process, but for $C_{20}Eu$, only one broad melting point can be seen (see the Supporting Information). Herein, we catch such a range of alkyl chain length where the mesophase of europium alkanoates emerges.

The overall enthalpy during the cooling process can be well plotted in a linear fitting with the number of CH_2 groups (see Figure 8). Fitting the enthalpy gives an intercept of -105.46 kJ mol^{-1} and a slope of 3.79 kJ (mol of CH_2)$^{-1}$. When the number of CH_2 groups is extrapolated to zero, the enthalpy may

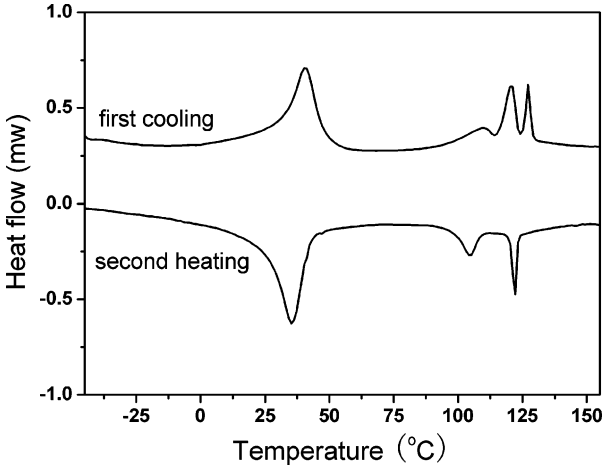

Figure 7. First cooling and second heating curves in DSC thermograms of $C_{16}Eu$.

TABLE 2: Transition Temperatures, Enthalpies, and Entropies of the Four Europium Alkanoates

	T_{trans}/°C		$\Delta_{trans}H$/kJ mol^{-1}		$\Delta_{trans}S$/J K^{-1} mol^{-1}	
n^a	reheating	cooling	reheating	cooling	reheating	cooling
14	22	18	23.1	24.4	78.3	83.7
	112	108	3.2	5.6	8.2	14.5
	125	125	6.3	4.2	15.8	10.6
	131		3.3		8.1	
16	40	35	35.4	40.4	112.9	131.0
	109	104	4.0	5.1	10.5	13.5
	120	122	6.0	4.0	15.3	10.2
	127		3.0		7.6	
18	49	42	3.0	1.8	5.5	5.6
	106	77	91.3	66.3	240.6	189.3
		94		6.2		17.0
20	117	88	108.4	99.5	277.5	275.6
		106		2.2		5.7

[a] n is the number of carbon atoms per chain.

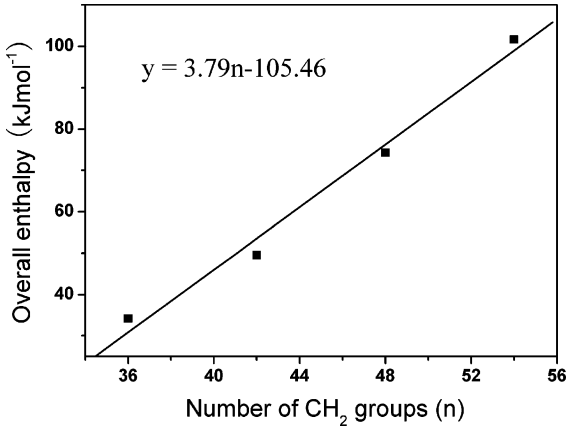

Figure 8. Linear fitting of overall enthalpy change (ΔH_{tot}) versus number of CH_2 groups ($r = 0.9926$).

be attributed to the electrostatic interactions between the carboxylate groups and the europium ions. Here, a negative value of intercept implies the electrostatic interactions contribute a negative effect to the melting. On the other hand, the slope reflects the fusion degree of the alkyl chains on heating. The larger value it is, the more complete fusion of the alkyl chains presents. For the present europium alkanoates, the slope of entropy change is similar to the value of 3.8 kJ (mol of CH_2)$^{-1}$ observed for the aliphatic chains from the fully crystalline state to complete fusion.[23] Compared with the corresponding fusion enthalpy of several lanthanide alkanoates, 3.45 kJ (mol of CH_2)$^{-1}$ for neodymium(III) alkanoates[18] and 2.5 kJ (mol of CH_2)$^{-1}$ for cerium(III) alkanoates,[2d] a regularity can be found that the enthalpy change per CH_2 group gradually increases with the increasing atomic number of the lanthanide, from cerium, neodymium, to europium. It has been reported that, for the alkanoates of lanthanide ions with smaller radii, lower melting points will result and the corresponding alkyl chains are more likely to melt completely.[2d] Therefore, the increasing enthalpy change of europium alkanoates should also arise from the decrease of europium ion radius.

From polarized optical microscopy, it is difficult to assign which liquid crystal phase these mesophases belong to, for good optical texture is hardly obtained. At room temperature, these compounds are opaque white powders and exhibit as black flakes under a polarized optical microscope. Upon heating, the powders become soft and begin to melt, and as a result, the black flakes gradually vanish from view. When the temperature ascends to the first phase transition point, all the compounds

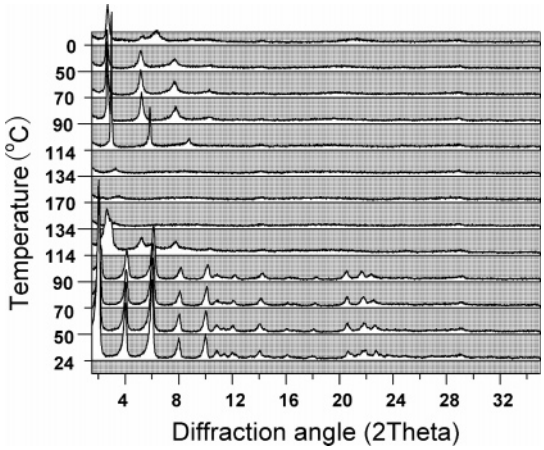

Figure 9. X-ray diffraction patterns of $C_{16}Eu$ at different temperatures upon heating and then cooling, from bottom to up.

become transparent liquids with high viscosities, which will maintain even if the temperature has risen to beyond the last melting point for 30−50 °C. Because of the high viscosity, these liquids are not very fluid and often contain many trapped air bubbles. The detailed common and polarized optical photographs that depict the process of melting can be seen in the Supporting Information. Unfortunately, we have not observed obvious birefringence of the mesophase even on cooling the isotropic liquids. The ambiguous texture and birefringence of lanthanide alkanoates have also been discussed in several reports.[2d,5,18] Therefore, for further clarifying the mesophase, temperature-dependent X-ray diffraction is employed to identify the mesophase of the compounds.

Figure 9 shows the X-ray diffraction patterns of $C_{16}Eu$ at different temperatures upon heating. At room temperature, the $C_{16}Eu$ exhibits a lamellar structure with a highly ordered intralayer conformation of alkyl chains. With the increase of temperature, the disorder of the alkyl chains begins to increase. As a result, the all-trans conformation of the alkyl chains is broken and the chains begin to soften until the final molten state. Therefore, the interlayer d spacing becomes smaller, as shown in Figure 10A. At the same time, the intralayer d spacing of alkyl chains increases due to the increasing degree of disordered conformation, as present in Figure 10B. Although the intralayer d spacing becomes larger and larger, the diffraction patterns at high angle about 20° are still distinct before the temperature has reached the first phase transition point, indicative of a certain order of alkyl chains being maintained. Once the $C_{16}Eu$ comes into the state of mesophase (114 °C), these diffractions at the high-angle region (about 22°) disappear, implying that the alkyl chains of intralayer have become highly disordered, similar to their liquid state. Meanwhile, the intralayer d spacing increases to its largest degree (see Figure 10B). However, the integral lamellar structure is not broken at this time, for strong progressional peaks in the low-angle range still exist. It is just such a coexistence of interlayer ordered and intralayer disordered structures that leads to the mesophase. In fact, the solid-to-mesophase transition can be considered the melting of alkyl chains, and the transition of the mesophase to isotropic liquid corresponds to destruction of the europium ionic layer.[18] Consequently, the structure of the mesophase can be comprehended as such a model: many disordered and liquidlike alkyl chains are hung on both sides of a toward-destructing plane of europium ions. Such a mesophase is similar to the smectic A phase, but it is not totally the same as observed for typical organic rodlike liquid crystals, because europium alkanotaes

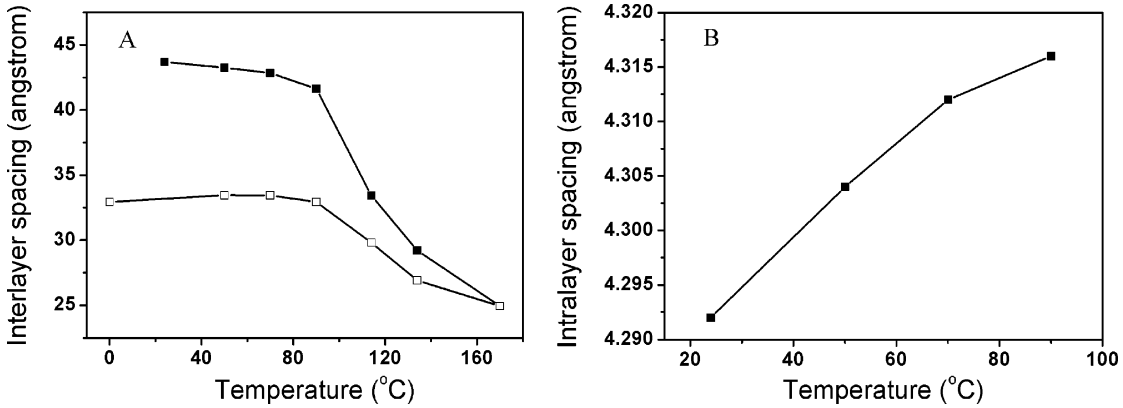

Figure 10. (A) Evolution of interlayer *d* spacing of $C_{16}Eu$ as a function of temperature from heating (■) to cooling (□). (B) Intralayer *d* spacing of $C_{16}Eu$ as a function of temperature on heating.

present the polymeric ionic layer mesophase rather than the discrete molecule mesophase.

On the basis of the model above, we can conclude that the mesophase of lanthanide alkanoates is mostly correlated to the thermal stability of the alkyl chains and the central metal ionic layer. The length of alkyl chains plays an important role in their thermal stability. The longer alkyl chains will bring stronger van der Waals interaction, thus leading to a higher melting point and an enhanced thermal stability. On the other hand, the radius of the lanthanide ion determines the interaction distance from the ion itself to the adjacent groups, and then further affects the electrostatic interaction among the ions themselves and the coordination interaction between the metal ions and the carboxylate groups. These interactions greatly affect the stability of the metal ionic layer. Therefore, the formation of the mesophase is finally attributed to two essential factors, the length of the alkyl chains and the radius of the metal ions, to which the latter has also been referred in Binnemans's work.[5]

Through this conclusion, the phenomena in our study can be explained rationally. It has been reported that the decreasing radius of lanthanide ions will cause decreasing distance between the carboxylate groups connected to both sides of the lanthanide ionic layer. Subsequently, the electrostatic repulsion between the carboxylate groups on opposite sides becomes stronger, making the ionic layer more unstable and more easily broken down upon heating. Thus, the alkanoates containing smaller lanthanide ions usually have lower melting points,[5] such as the heavier lanthanide alkanoates. For such alkanoates, longer alkyl chains are required to contribute more intermolecular interactions to maintain the whole lamellar structure to avoid destruction during the heating process. Once the supplemental intermolecular interactions grow to be equivalent with the instability of the ionic layer, the destruction of the whole bilayer structure will be held back and a mesophase will form, just as in the present case.

During the cooling process, liquid $C_{16}Eu$ solidifies into a glassy state, unlike its initial loose powders. Even on cooling to 0 °C, the X-ray diffraction patterns in the high-angle region do not appear again, indicative of the original intralayer structure unresumed. Meanwhile, the interlayer *d* spacing is also much smaller than the one before heating (see Figure 10B). However, FT-IR spectra show the alkyl chains after the heating process still remain in a well-ordered conformation, for the antisymmetric and symmetric stretching modes of CH_2 reappear at 2918 and 2949 cm^{-1}, respectively. Therefore it seems that the alkyl chains may have folded during the heating process.[18] All four samples are a similar case. The transition to glassy state of metal soaps after heating is a common phenomenon and has been reported elsewhere.[2d]

Conclusion

Through simple precipitation from the solution, europium alkanoates $C_{14}Eu$, $C_{16}Eu$, $C_{18}Eu$, and $C_{20}Eu$ can self-assemble into multibilayer structures, in which the all-trans alkyl chains are perpendicular to the central europium ionic layers. Inside such bilayers, the highly ordered alkyl chains arrange compactly and are in a state of similar hexagonal packing. At the heads of the chains, there is a mixed-coordination type of chelating and bridging bidentate between the carboxylate groups and the europium ions. All the samples exhibit a characteristic emission of europium, although the luminescent intensity is weakened due to the quench of the carboxylate groups. Different from the previous europium dodecanoate with a single melting point, the present europium alkanoates show obvious mesophases on heating. For the lanthanide alkanoates of higher atomic number, the decreasing radius of the central ion results in the decreased stability of the central ionic layer on heating. However, the decreased stability can be compensated by the increased interactions between the alkyl chains with larger lengths. Once the compensation is equivalent to the instability, a mesophase will occur. Thus, there should be such a tendency: the higher atomic number the lanthanide belongs to, the longer alkyl chains of their alkanoates are required to form the mesophase on heating. Future work will focus on the following two areas: one is introducing suitable mesogens to the alkyl chains to lower the temperature of the meosphase down to a practical range, and the other is trying to replace the carboxylate groups by ligands of weaker quenching ability, such as sulfonic groups, to gain a more intense luminescence.

Acknowledgment. The authors acknowledge financial support from the National Natural Science Foundation of China (Grant 20473032), the Major State Basic Research Development Program (Grant G2000078102), the PCSIRT of the Ministry of Education of China, and the Innovation Fund of Jilin University. The authors thank for Ms. Shuyun Wang (Changchun Institute of Applied Chemistry) for her help in the measurement of temperature-dependent XRD.

Supporting Information Available: Fluorescence spectra, entropy change (ΔS_{tot}) versus number of CH_2 groups, common and polarized optical photos of all samples, DSC thermograms of $C_{14}Eu$, $C_{18}Eu$, and $C_{20}Eu$, and FT-IR spectra of $C_{16}Eu$ before

and after heating. This material is available free of charge via the Internet at http://pubs.acs.org.

References and Notes

(1) (a) Ulman, T. *Chem. Rev.* **1996**, *96*, 1533. (b) Love, J. C.; Wolfe, D. B.; Haasch, R.; Chabinyc, M. L.; Paul, K. E.; Whitesides, G. M.; Nuzzo, R. G. *J. Am. Chem. Soc.* **2003**, *125*, 2597. (c) Bensebaa, F.; Ellis, T. H.; Kruus, E.; Voicu, R.; Zhou, Y. *Langmuir* **1998**, *14*, 6579. (d) Bu, W.; Fan, H.; Wu, L.; Hou, X.; Hu, C.; Zhang, G.; Zhang, X. *Langmuir* **2002**, *18*, 6398.

(2) (a) Pradeep, T.; Sandhyarani, N. *J. Mater. Chem.* **2001**, *11*, 1294. (b) Baena, M. J.; Espinet, P.; Lequerica, M. C.; Levelut, A. M. *J. Am. Chem. Soc.* **1992**, *114*, 4182. (c) Fijolek, H. G.; Grohal, J. R.; Sample, J. L.; Natan, M. J. *Inorg. Chem.* **1997**, *36*, 622. (d) Marques, E. F.; Burrows, H. D.; da Graca Miguel, M. *J. Chem. Soc., Faraday Trans.* **1998**, *94*, 1729.

(3) (a) Baena, M. J.; Espinet, P.; Lequerica, M. C.; Levelut, A. M. *J. Am. Chem. Soc.* **1992**, *114*, 4182. (b) Espinet, P.; Esteruelas, M. A.; Oro, L. A.; Serrano, J. L.; Sola, E. *Coord. Chem. Rev.* **1992**, *117*, 215. (c) Binnemans, K.; Heinrich, B.; Guillon, D.; Bruce, D. W. *Liq. Cryst.* **1999**, *26*, 1717. (d) Jongen, L.; Hinz, D.; Meyer, G.; Binnemans, K. *Chem. Mater.* **2001**, *13*, 2243.

(4) (a) Binnemans, K.; Gorller-Walrand, C. *Chem. Rev.* **2002**, *102*, 2303. (b) Binnemans, K.; Jongen, L.; Görller-Walrand, C. *Phys. Chem. Chem. Phys.* **2001**, *3*, 4796.

(5) Binnemans, K.; Jongen, L.; Gorller-Walrand, C.; D'Olieslager, W.; Hinz, D.; Meyer, G. *Eur. J. Inorg. Chem.* **2000**, 1429.

(6) Rueff, J.-M.; Masciocchi, N.; Rabu, P.; Sironi, A.; Skoulios, A. *Chem.*−*Eur. J.* **2002**, *8*, 1813.

(7) (a) Walczak, M. M.; Chung, C.; Stole, S. M.; Widrig, C. A.; Porter, M. D. *J. Am. Chem. Soc.* **1991**, *113*, 2370. (b) Tao, Y. T. *J. Am. Chem. Soc.* **1993**, *115*, 4350. (c) MacPhail, R. A.; Strauss, H. L.; Snyder, R. G.; Elliger, C. A. *J. Phys. Chem.* **1984**, *88*, 334. (d) Senak, L.; Moore, D.; Mendelsohn, R. *J. Phys. Chem.* **1992**, *96*, 2749.

(8) (a) Snyder, R. G.; Strauss, H. L.; Elliger, C. A. *J. Phys. Chem.* **1982**, *86*, 5145. (b) Snyder, R. G.; Maroncelli, M.; Strauss, H. L.; Hallmark, V. M. *J. Phys. Chem.* **1986**, *90*, 5623.

(9) Parikh, A. N.; Gillmor, S. D.; Beers, J. D.; Beardmore, K. M.; Cutts, R. W.; Swanson, B. I. *J. Phys. Chem. B* **1999**, *103*, 2850.

(10) Weers, J. G.; Scheuing, D. R. In *Fourier Transfrom Infrared Spectrosxopy in Colloid and Interface Science*; Scheuing, D. R., Ed.: American Chemical Society: Washington, DC, 1991; p 91.

(11) Ren, Y.; Iimura, K.-I.; Ogawa, A.; Kato, T. *J. Phys. Chem. B* **2001**, *105*, 4305.

(12) Snyder, R. G. *J. Mol. Spectrosc.* **1961**, *7*, 117.

(13) Nielsen, J. R.; Hathaway, R. G. *J. Mol. Spectrosc.* **1963**, *10*, 336.

(14) Meiklejohn, R. A.; Meyer, R. J.; Aronovic, S. M.; Schuette, H. A.; Meloch, V. W. *Anal. Chem.* **1957**, *29*, 329.

(15) Kirby, E. M.; Evans-Vader, M. J.; Brown, M. A. *J. Am. Oil Chem. Soc.* **1965**, *42*, 437.

(16) Lin-Vien, D.; Colthup, N. B.; Fateley, W. G.; Grasselli, J. G. *Infrared and Raman Characteristic Frequencies of Organic Molecules*; Academic Press: San Diego, CA, 1991; pp 137−140.

(17) Nakamoto, K. *Infrared and Raman spectra of Inorganic and Coordination Compounds*; Wiley: New York, 1986.

(18) Binnemans, K.; Jongen, L.; Bromant, C.; Hinz, D.; Meyer, G. *Inorg. Chem.* **2000**, *39*, 5938.

(19) Ofelt, G. S. *J. Chem. Phys.* **1963**, *38*, 2171.

(20) Yamase, T.; Kobayashi, T.; Sugeta, M.; Naruke, H. *J. Phys. Chem. A* **1997**, *101*, 5046.

(21) (a) Bu, W.; Li, H.; Li, W.; Wu, L.; Zhai, C.; Wu, Y. *J. Phys. Chem. B* **2004**, *108*, 12776. (b) Sugeta, M.; Yamase, T. *Acta Crystallogr.* **1997**, *C53*, 1166. (c) Corkery, R. W.; Martin, J. P. D. *J. Lumin.* **1999**, *82*, 1.

(22) (a) Blasse, G.; Schipper, W.; Hamelink, J. J. *Inorg. Chim. Acta* **1991**, *189*, 77. (b) Frey, S. T.; Horrocks, W. DeW., Jr. *Inorg. Chem.* **1991**, *30*, 1073.

(23) Seurin, P.; Guillon, D.; Skoulios, A. *Mol. Cryst. Liq. Cryst.* **1981**, *65*, 85.